VIP Supramolecular Chemistry

DOI: 10.1002/ange.201303083

Stepwise-Resolved Thermodynamics of Hydrophobic Self-Assembly**

Alina Grego, Achim Müller, and Ira A. Weinstock**

Dedicated to Professor François Diederich on the occasion of his 60th birthday

Hydrophobic effects refer to energetically favorable associations of nonpolar molecules in water.[1] These effects are responsible for numerous processes in chemistry and biology, including micelle[2] and lipid-bilayer formation,[3] protein folding,[4] assembly[5] and aggregation,[6] substrate binding,[7] and host/guest encapsulation.[8] In general, the energetic phenomena responsible for hydrophobic assembly include changes in entropy and enthalpy associated with hydrophobic solvation,[9] the release of water from nanoscale hydrophobic domains,[5,10] and van der Waals interactions[7d] between nonpolar components in compactly organized structures.

Among numerous types of hydrophobically assembled structures, micelles are viewed as fundamentally important products of surfactant aggregation processes,[2–3,11] which could serve as useful models for understanding multistep hydrophobic assembly. Indeed, numerous studies[2] do report the entropy and enthalpy changes that determine critical micelle concentrations (CMCs).[12] Data from these investigations typically reveal classical thermodynamic signatures involving (net) increases in entropy. However, once the CMC is reached, micelle formation is rapid and spontaneous, such that, even for the special case of micelle formation, very little experimental data is available concerning the energetics of individual growth steps. We now address this challenging fundamental problem by using an unprecedented type of experiment that gives rise to a structurally well-defined micelle-like organic aggregate of *n*-butyrate ions within a porous inorganic-oxide nanocapsule. This access to detailed information concerning the evolving influences of different hydrophobic effects associated with numerous individual assembly steps has never been achieved, despite over a century of fundamental studies of surfactant aggregation.

The nanocapsule is a $(pentagon)_{12}(linker)_{30}$-type anionic complex, $[\{Mo^{VI}{}_6O_{21}(H_2O)_6\}_{12}\{(Mo^{V}{}_2O_4)_{30}(acetate)_{22}(H_2O)_{16}\}]^{34-}$,[13] abbreviated as $[\mathbf{1}(acetate)_{22}(H_2O)_{16}]^{34-}$, where **1** refers to the inorganic capsule framework. A cutaway view of the capsule is shown in Figure 1, left.

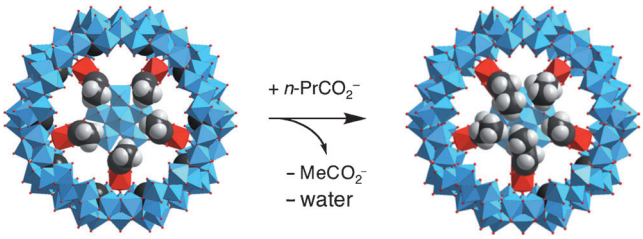

Figure 1. Cutaway views illustrating the replacement of five acetates by larger *n*-butyrate ligands (a maximum of 24 can fit inside the complex) with loss of water from the interior of the capsule.

This capsule is a derivative of a nanocontainer with 30 acetate ligands[13c] that has been employed in recent years for studies related to aspects of materials science.[14] Its metal-oxide skeleton is comprised of 12 $\{(Mo)Mo_5\}$-type pentagons and 30 linkers, whose structural organization gives rise to 20 metal-oxide $\{Mo_9O_9\}$ rings that provide access to the interior of the soluble capsule. In aqueous solution, these $\{Mo_9O_9\}$ pores are flexible,[13b] allowing for rapid equilibration between carboxylate ligands in bulk solution outside the complex, and those suspended/hanging from the Mo^V centers inside the capsule. The related 30 $\{Mo^{V}{}_2O_4\}^{2+}$ linkers ($\{Mo^{v}{}_2\}$), which span a truncated icosahedron,[13a,14] have a directing influence on different types of hydrophobic assemblies inside the capsule because they provide 30 geometrically fixed positions, each of which weakly binds either a single bidentate carboxylate anion, or two water molecules.

The weakly bound acetate ions of the $[\mathbf{1}(acetate)_{22}(H_2O)_{16}]^{34-}$ capsule, and approximately 35 unbound water molecules (not shown in the formula), are displaced in a stepwise fashion by the controlled uptake of from one to 24 *n*-butyrate ions, giving a micelle-like $(n\text{-butyrate})_{24}$ assembly[15] with a practically water-free[16] central cavity (Figure 1, right). This should be compared to the aggregation of *n*-butyric acid in aqueous solution, where large (3.5 M) concentrations of the short-chain fatty acid[17] give rise to micelles comprised of approximately 80 of the amphiphilic components.[18] In contrast to assembly in bulk media, however, the porous capsule makes it possible to investigate

[*] A. Grego, Prof. I. A. Weinstock
Department of Chemistry and the Ilse Katz Institute for Nanoscale Science and Technology, Ben Gurion University of the Negev
Beer Sheva, 84105 (Israel)
E-mail: iraw@bgu.ac.il
Homepage: http://www.bgu.ac.il/~iraw/Home.html
Prof. A. Müller
Fakultät für Chemie, Universität Bielefeld
Postfach 100131, 33501 Bielefeld (Germany)
E-mail: a.mueller@uni-bielefeld.de
Homepage: http://www.uni-bielefeld.de/chemie/ac1/

[**] I.A.W. and A.M. thank the Deutsche Forschungsgemeinschaft and A.G. the Kreitman Foundation for support. A.M. thanks the ERC (Brussels) for an Advanced Grant. We also thank Dr. Hugo Gottlieb, Dr. Keren Adamsky, and Dr. Jordan Chill for assistance with 2D NMR spectroscopy, Dr. Irina Shin for assistance with ITC, Sivil Kopilevich, Dr. Pere Miro and Dr. Alice Merca for graphics, and Dr. Boris Rybtchinski for comments.

Supporting information for this article is available on the WWW under http://dx.doi.org/10.1002/anie.201303083.

the underlying energetics associated with each step in the formation of the 24 *n*-butyrate assembly within the inorganic framework of **1**.

Direct evidence for the controlling role of hydrophobic effects in the uptake of *n*-butyrate ions by **1** was provided by competitive encapsulation of differently sized carboxylate ions (Supporting Information, Figure S1). A dramatic preference for replacement of acetate by carboxylate ions with larger *n*-alkyl R groups (Et and *n*Pr) is observed, whereas the small variations in the pK_a values of the carboxylate ions show no correlation with preferential encapsulation, which increases in the order: R (pK_a) = CH_3 (4.76) < Et (4.88) ≪ *n*-Pr (4.82). Hence, the preferential encapsulation of *n*-butyrate ions (R = *n*Pr) by **1** is primarily due to hydrophobic effects[19] arising from the two additional -CH_2- groups in the *n*-butyrate anions (in combination with a much smaller charge/volume ratio).

A unique set of experiments was then used to reveal the evolving roles of enthalpy and entropy associated with the step-wise encapsulation of *n*-butyrate ions (Figure 2).

To begin (Figure 2a), ^{1}H NMR spectroscopy was used to determine the numbers of equivalents of *n*-butyrate encapsulated by **1** as the total concentration of this anion was incrementally increased. First, acetate buffer (20 equiv) was added to bring the number of internally bound acetate ligands to 28.1 ± 0.2, representing near saturation of the {Mo^V_2} binding sites. Then, in separate NMR-tube reactions, incrementally larger amounts of *n*-butyrate buffer were added. After adding 3.1 equivalents of *n*-butyrate, an average of 2.3 equivalents were located inside the capsule and 0.8 equivalents remained in the bulk solution (Figure 2a, lower spectrum). After 16.3 equivalents were added, 14.8 *n*-butyrate ions were encapsulated, leaving only 1.5 equivalents in the bulk solution (Figure 2a, upper spectrum). The selective uptake of *n*-butyrate is evident from the large increase in intensity of the ^{1}H NMR signals arising from the -CγH_3 endgroups of the internally bound ligands (−0.5 to −0.8 ppm), which is accompanied by a much smaller increase in intensity of the well-resolved multiplets at 1.4 and 2.2 ppm that are assigned to the -C$_\beta H_2$- and -C$_\alpha H_2$- groups, respectively, of *n*-butyrate in bulk solution.

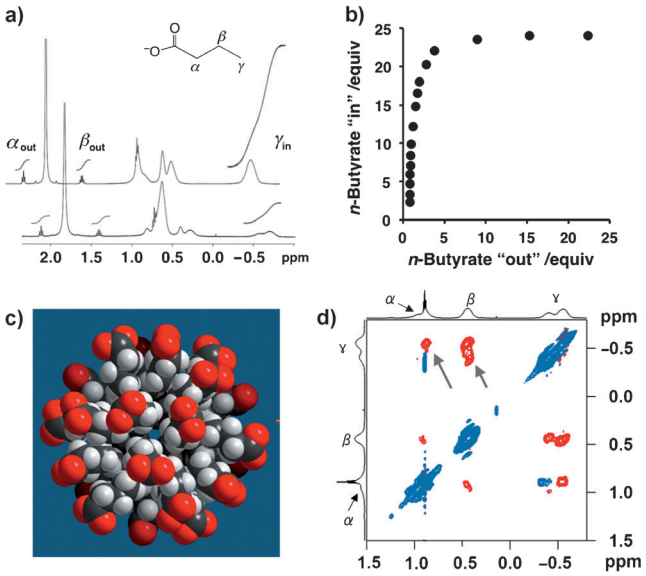

Figure 2. Hydrophobic self-assembly of *n*-butyrate ions inside the porous molybdenum-oxide capsule **1**. a) ^{1}H NMR spectra (with indicated signal intensities at the same scale) after addition of 3.1 equiv (bottom) and 16.3 equiv (top) of *n*-butyrate buffer to [**1**(acetate)$_{28}$-(H_2O)$_4$]$^{40-}$ in D_2O. The broad signals at ca. −0.7 ppm are due to the methyl protons on the γ-carbon atoms of internally bound *n*-butyrate ions. b) Equivalents of encapsulated *n*-butyrate ions ("in") as a function of those remaining in bulk solution ("out") after uptake by the capsule. c) Space-filling model of the (*n*-butyrate)$_{24}$ assembly/micelle encapsulated within the metal-oxide skeleton of **1**, according to a single-crystal X-ray crystallography study;[15] O red, C black), H grey. d) Two-dimensional ROESY NMR spectrum of a capsule containing two encapsulated *n*-butyrate ions, along with ca. 26 internal (^{1}H NMR silent) [D_3]acetate ligands, $CD_3CO_2^-$. Negative ROE cross-peaks are shown as red contours, relative to the positive diagonal peaks in dark blue. The leftmost grey arrow at the top of the Figure corresponds to interactions between C–H bonds on α- and γ-carbon atoms, and the grey arrow at its right corresponds to interactions between C–H bonds on β- and γ-carbon atoms.

The data from the complete series of ^{1}H NMR experiments (Figure S2) are plotted in Figure 2b. As more *n*-butyrate ions are added, the numbers of equivalents located inside **1** climb steeply at first, while the numbers of equivalents left in the bulk solution remain remarkably small. This occurs despite a large excess of acetate buffer (48 equivalents in all), which reflects the pronounced preference for encapsulation of *n*-butyrate over acetate ligands.

The number of internally-fixed *n*-butyrate ions reaches a maximum value of 24, which is identical to the number found in the X-ray crystallography study mentioned above.[15] Once encapsulated within **1**, the carboxylate groups of the *n*-butyrate ions point outwards, giving a beautiful/unique structure similar to that of micelles (Figure 2c). However, rather than forming ion pairs with hydrated countercations (as is typical for micelles), the carboxylate end groups are associated with the {Mo^V_2} linkages of the metal-oxide framework of **1** (omitted for clarity in Figure 2c). This rather compact and symmetrical *n*-butyrate-type structure is strongly favored over the encapsulation of acetate ions, which cannot show significant hydrophobic effects or compact structures. Importantly, few, if any, water molecules are present in the hydrophobic center of the "micelle" in Figure 2c. Rather, an approximately 11 Å diameter void space is formed, surrounded by 72 H atoms from -CγH_3 endgroups of the 24 *n*-butyrate ions. This observation is of general importance for protein and related ligand–drug interaction research, because of the relationship between the sizes of hydrophobic protein pockets and numbers of encapsulated water molecules: sufficiently small hydrophobic cavities do not contain water.[7d,10b,20]

Consistent with a hydrophobically driven self-assembly of *n*-butyrate ions inside **1**, 2D ROESY NMR data reveal close contacts between H atoms from C–H bonds on adjacent *n*-Pr groups when as few as two molecules of *n*-butyrate (on average) are present inside each capsule (Figure 2d; see Figure S3 for the full spectrum). Because the cross peaks assigned to interactions between *n*-butyrate ions are broad and close to the chemical-shift values of internally bound acetate, a capsule containing $CD_3CO_2^-$ ligands was prepared to eliminate any ambiguity in peak assignments (see the

Supporting Information for synthesis details). Hence, all observed signals are due to the n-butyrate ions alone, and the red-colored ROE cross-peaks are unequivocally assigned to intermolecular interactions between C–H bonds of encapsulated *n*-butyrate ions. The observation of intermolecular interactions when only two *n*-butyrate ions are present inside the capsule confirms that the successful competition of *n*-butyrate (relative to acetate) for encapsulation by **1** is due to a hydrophobic effect (involving the exclusion of water) arising from the two additional methylene groups in *n*-butyrate. We then determined the equilibrium constants associated with sequential steps in the formation of the *n*-butyrate assembly.

The first task was to demonstrate that the *n*-butyrate-type capsule system is at equilibrium based on dynamic ligand exchange. This was done by approaching a common position of equilibrium from opposite directions: by adding *n*-butyrate buffer to a solution of $[\mathbf{1}(\text{acetate})_{28}(D_2O)_4]^{40-}$, and acetate buffer to a solution of $[\mathbf{1}(n\text{-butyrate})_{24}(D_2O)_{12}]^{36-}$. After two minutes at 23 °C, the nature and ^{1}H NMR signal intensities of species inside and outside **1** in both experiments were effectively identical, thus confirming thermodynamic control (Figure S4).

To obtain equilibrium constants (*K*) for sequential growth steps, a mass-balance expression must be defined for each successive ligand-exchange reaction. By design, each ligand-exchange reaction involved 1:1 displacements of internally bound acetates by *n*-butyrate ligands, such that the total number of carboxylate ligands inside **1** remained constant. This is shown in Figure 3a, where the slope of the line

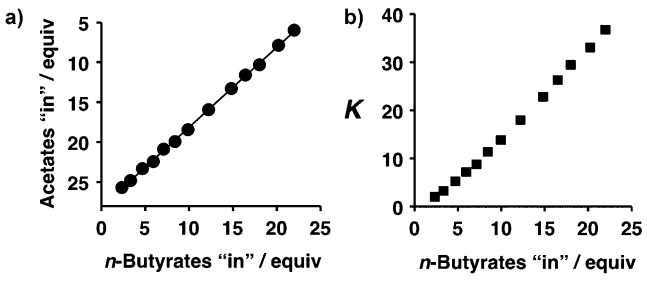

Figure 3. One-to-one displacement of acetate by *n*-butyrate ions inside the capsule with the skeleton of **1**, and (dimensionless) equilibrium constants (*K*) for the sequential uptake of incrementally more *n*-butyrate ligands. a) Equivalents of internally bound acetate ions as the number of encapsulated *n*-butyrate ions increases from two to near completion (for the first 13 data points in Figure 2b). b) Equilibrium constants for each degree of *n*-butyrate-ion encapsulation in (a).

obtained by linear regression is 0.99, which is diagnostic for a 1:1 replacement of acetate by *n*-butyrate at each step of the self-assembly process. As such, the equilibrium constant for *n*-butyrate ion uptake at each concentration of added *n*-butyrate buffer was calculated using a simple mass-balance expression for 1:1 ligand exchange.[21] Remarkably, the equilibrium constants (23 °C) increase by over an order of magnitude as more *n*-butyrate ions become encapsulated (Figure 3b). For encapsulation of the first two ions (for which 2D ROESY NMR spectra show pair-wise[22] interactions), the equilibrium constant is a modestly favorable value of 1.5. Subsequent growth steps become significantly more favorable, with *K* reaching a value of 36.6 for the nearly completed micelle-like structure.

This thermodynamically cooperative[23] behavior may explain why multi-component hydrophobic self-assembly processes typically proceed finally to complete (compact) assemblies, rather than to mixtures of intermediate and final structures. A good example in the present context is micelle formation: once the critical micelle concentration (CMC) is reached, only completed micelles are typically observed. Hence, investigation of the energetics of the numerous sequentially related equilibrium constants associated with each individual step in micelle formation is simply not feasible. Access to such information is now possible, however, by investigating the step-wise formation of the (n-butyrate$_{24}$) assembly within the well-defined metal-oxide skeleton of **1**.

To reveal the thermodynamic signatures of these individual steps, the temperature dependence of the equilibrium constants plotted in Figure 3b, were determined by ^{1}H NMR spectroscopy (from 283–333 K; Figure S5). Plots of $\ln K$ versus T^{-1} (Figure S6) then revealed the enthalpy ($\Delta H°$) and entropy ($\Delta S°$) changes associated with each degree of assembly. In Figure 4a, values of $\Delta H°$, $-T\Delta S°$, and Gibbs free energies ($\Delta G°$) are plotted in kcal mol^{-1} as functions of the numbers of *n*-butyrate ions present inside **1**.

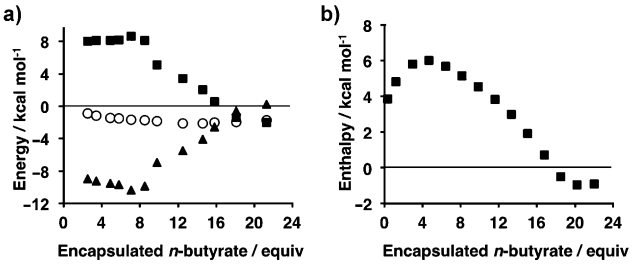

Figure 4. Enthalpic ($\Delta H°$; ■) and entropic ($-T\Delta S°$; ▲) contributions to the Gibbs free energies ($\Delta G°$; ○) at 295 K during stepwise self-assembly of *n*-butyrate anions inside the capsule with the skeleton of **1**. a) Values (in kcal mol^{-1}) for capsules containing the numbers of internally bound *n*-butyrate ions indicated on the x axis. Statistical uncertainties in $\Delta H°$ and $\Delta S°$ are ± 0.2 and ± 0.3 kcal mol^{-1}, respectively. b) Enthalpies (■) for the same incremental steps in (a), but obtained directly from heat values measured by isothermal titration calorimetry (ITC; at (298 ± 0.1) K) in water.

Early in the self-assembly, entropy changes ($\Delta S°$) are positive, giving strongly favorable energies (negative values of $-T\Delta S°$ at 295 K) of ca. −8.5 kcal mol^{-1}, which become more favorable as the assembly grows from a few *n*-butyrate ions to approximately one third of its final size. During this phase, the favorable entropy changes associated with removal of the hydrophobic ions from bulk water are partially offset by unfavorable changes in enthalpy ($\Delta H°$).[9] This is a classic thermodynamic signature, originally derived from studies of hydrocarbon dissolution in water, and encountered in numerous investigations of hydrophobic effects.[1a] Accordingly, the entropic costs imposed on water by the hydrocarbon chain of the *n*-butyrate ion are larger in bulk solution than in the

uniquely hydrated microenvironment inside the capsule. Meanwhile, the positive (unfavorable) change in enthalpy associated with encapsulation of the *n*-butyrate anion shows that hydrophobic solvation is less effective inside the capsule than it is in bulk solution.

As the structure grows, the thermodynamic signatures of successive steps undergo a smooth reversal, leading finally to an enthalpically driven late-growth phase close to completion of the micelle-like aggregate. This important result was independently confirmed by using isothermal titration calorimetry (ITC, see Figure S7) to directly measure the heat (molar change in enthalpy) associated with each step in Figure 4a. The ITC data (Figure 4b) show that early steps in the assembly are associated with unfavorable increases in enthalpy. These gradually decrease with continued aggregate formation until, in the final stages, individual growth steps become exothermic. Despite the use of two entirely different techniques (ITC data and van't Hoff plots obtained from variable-temperature ^{1}H NMR spectra), analogous and quantitatively similar results were obtained.

The single-crystal X-ray structure of the crystalline compound containing the of skeleton **1** with the $(n\text{-butyrate})_{24}$ assembly (Figure 2c)[15] is notable for the ca. 11 Å diameter hydrophobic cavity formed in the central part of the capsule.[10b] To reach this final condition, water molecules in the interior of the capsule must be incrementally displaced, most likely during latter stages of the *n*-butyrate assembly. Although the release of nano-confined water could contribute to favorable enthalpy changes,[7a–c] the formation of an increasingly water-depleted hydrophobic region inside the capsule sets the stage for dispersion forces to eventually dominate the net-enthalpy changes associated with encapsulations of *n*-butyrate ions (analogous to hydrophobic substrates in dry protein binding sites[7d,24]). This explains why, after encapsulation of ca. 16 *n*-butyrate ions (see Figure 4), further growth inside the capsule is dominated by favorable (negative) enthalpy changes.

As the values for the stepwise changes in enthalpy gradually shift from positive to negative (from endo- to exothermic), the entropy changes ($\Delta S°$) associated with each step become less favorable. These eventually reach values near zero as the entropic driving force for removal of *n*-butyrate ions from bulk water is increasingly offset by entropically unfavorable losses in configurational degrees of freedom associated with completion of the rather compact assembly of *n*-butyrate ions inside the capsule. These gradual shifts in the entropy and enthalpy changes associated with sequential steps lead to the reversal of their respective roles, as shown in Figure 4. Remarkably, this transition occurs smoothly, with the equilibrium constants and associated Gibbs free energies for successive steps (Figures 3b and 4a) providing no indication whatsoever of the underlying hand-off between entirely different types of hydrophobic effects.

Finally, the (net) entropy and enthalpy changes per mole of $(n\text{-butyrate})_{22}$ formation (22 out of 24 *n*-butyrates[25]) were determined by integrating the areas under the plots in Figure 4a. The overall assembly process is entropically favorable ($-T\Delta S°_{total}$ = ca. -112 kcal mol^{-1} at 295 K), with a smaller unfavorable change in enthalpy ($\Delta H°_{total}$ = ca. $+81$ kcal mol^{-1}), giving a total Gibbs free energy ($\Delta G°_{total}$) of ca. -31 kcal mol^{-1}. Although the overall process is entropically driven, this dominant thermodynamic signature masks the important role of enthalpy as the formation of the micelle-like structure approaches its completion. This demonstrates how the final steps in formation, as well as in the self-repair, of hydrophobically stabilized structural domains, such as those in folded and aggregated proteins, and lipid-bilayer membranes, can in fact be enthalpically driven, even if the overall formation of these assemblies is due to favorable (net) changes in entropy.

In conclusion, the unique experimental method introduced herein provides an unprecedented step-by-step picture of how diverse energetic influences, collectively termed hydrophobic effects, act in a seamlessly concerted fashion to drive a spontaneous progression from initial pairwise interactions between amphiphillic molecules to formation of a micelle-like aggregate with a water-depleted central cavity. This versatile method promises new access to information concerning intermediate stages of biologically related and other important hydrophobic assembly processes, with the option for extension based on the present capsule.

Received: April 12, 2013
Published online: June 13, 2013

Keywords: butyrates · hydrophobic effect · nanocapsules · self-assembly · thermodynamics

[1] a) W. Blokzijl, J. B. F. N. Engberts, *Angew. Chem.* **1993**, *105*, 1610–1650; *Angew. Chem. Int. Ed.* **1993**, *32*, 1545–1579; b) P. Ball, *Chem. Rev.* **2008**, *108*, 74–108.

[2] C. Tanford, *The hydrophobic effect: Formation of micelles and biological membranes*, 2nd ed., Wiley, New York, **1980**.

[3] P. Nelson, *Biological Physics: Energy, Information, Life*, W. H. Freeman & Co., New York, **2008**.

[4] K. A. Dill, J. L. MacCallum, *Science* **2012**, *338*, 1042–1046.

[5] P. Liu, X. Huang, R. Zhou, B. J. Berne, *Nature* **2005**, *437*, 159–162.

[6] D. Thirumalai, G. Reddy, J. E. Straub, *Acc. Chem. Res.* **2012**, *45*, 83–92.

[7] a) A. Biela, N. N. Nasief, M. Betz, A. Heine, D. Hangauer, G. Klebe, *Angew. Chem.* **2013**, *125*, 1868–1876; *Angew. Chem. Int. Ed.* **2013**, *52*, 1822–1828; b) P. W. Snydera, J. Mecinovi, D. T. Moustakasa, A. W. Thomas III, M. Hardera, E. T. Macka, M. R. Locketta, A. Hérouxb, W. Shermanc, G. M. Whitesides, *Proc. Natl. Acad. Sci. USA* **2011**, *108*, 17889–17894; c) M. Ellermann, R. Jakob-Roetne, C. Lerner, E. Borroni, D. Schlatter, D. Roth, A. Ehler, M. G. Rudolph, F. Diederich, *Angew. Chem.* **2009**, *121*, 9256–9260; *Angew. Chem. Int. Ed.* **2009**, *48*, 9092–9096; d) E. Barratt, R. J. Bingham, D. J. Warner, C. A. Laughton, S. E. V. Phillips, S. W. Homans, *J. Am. Chem. Soc.* **2005**, *127*, 11827–11834.

[8] a) J.-M. Lehn, *Supramolecular Chemistry: Concepts and Perspectives*, VCH, Weinheim, **1995**; b) D. Ajami, J. Rebek, *Acc. Chem. Res.* **2013**, *46*, 990–999.

[9] B. N. Solomonov, I. A. Sedev, *J. Phys. Chem. B* **2006**, *110*, 9298–9303.

[10] a) T. A. Pascal, W. A. Goddard, J. Yousung, *Proc. Natl. Acad. Sci. USA* **2011**, *108*, 11794–11798; b) S. Sharma, P. G. Debenedetti, *Proc. Natl. Acad. Sci. USA* **2012**, *109*, 4365–4370.

[11] B. Alberts, A. Johnson, J. Lewis, M. Raff, K. Roberts, P. Walter, *Molekularbiologie der Zelle*, 4th ed., Wiley-VCH, Weinheim, **2004**.
[12] J. Lah, C. Pohar, G. Vesnaver, *J. Phys. Chem. B* **2000**, *104*, 2522 – 2526.
[13] a) S. Kopilevich, A. Gil, M. Garcia-Ratés, J. B. Avalos, C. Bo, A. Müller, I. A. Weinstock, *J. Am. Chem. Soc.* **2012**, *134*, 13082 – 13088; b) A. Ziv, A. Grego, S. Kopilevich, L. Zeiri, P. Miro, C. Bo, A. Müller, I. A. Weinstock, *J. Am. Chem. Soc.* **2009**, *131*, 6380 – 6382; c) A. Müller, S. K. Das, E. Krickemeyer, C. Kuhlmann, M. Sadakane, M. H. Dickman, M. T. Pope, *Inorg. Synth.* **2004**, *34*, 191 – 200.
[14] A. Müller, P. Gouzerh, *Chem. Soc. Rev.* **2012**, *41*, 7431 – 7463.
[15] C. Schäffer, H. Bögge, A. Merca, I. A. Weinstock, D. Rehder, E. T. K. Haupt, A. Müller, *Angew. Chem.* **2009**, *121*, 8195 – 8200; *Angew. Chem. Int. Ed.* **2009**, *48*, 8051 – 8056.
[16] Based on the X-ray structural data in Ref. [15], it is difficult to rule out the possibility that a small number of crystallographically disordered water molecules might be present in the ca. 1330 $Å^3$ volume of the central hydrophobic cavity; see: B. W. Matthews, L. Liu, *Protein Sci.* **2009**, *18*, 494 – 502.
[17] *n*-Butyric acid, a short-chain fatty acid, plays a role in important biochemical and patho-biochemical processes: J. R. Lupton, *J. Nutr.* **2004**, *134*, 479 – 482.
[18] M. Davies, D. M. L. Griffiths, *Z. Phys. Chem.* **1956**, *6*, 143 – 150.
[19] C. Schäffer, A. M. Todea, H. Bögge, O. A. Petina, D. Rehder, E. T. K. Haupt, A. Müller, *Chem. Eur. J.* **2011**, *17*, 9634 – 9639.
[20] L. Wang, B. J. Berne, R. A. Friesner, *Proc. Natl. Acad. Sci. USA* **2011**, *108*, 1326 – 1330.
[21] $K = ([n\mathrm{Bu}]_{\mathrm{inside}} \times [\mathrm{acetate}]_{\mathrm{outside}})/([n\mathrm{Bu}]_{\mathrm{outside}} \times [\mathrm{acetate}]_{\mathrm{inside}})$.
[22] a) G. Kegeles, *J. Phys. Chem.* **1979**, *83*, 1728 – 1732; b) I. Portnaya, R. Khalfin, E. Kesselman, O. Ramon, U. Cogana, D. Danino, *Phys. Chem. Chem. Phys.* **2011**, *13*, 3153 – 3160.
[23] J. F. Douglas, J. Dudowicz, K. F. Freed, *J. Chem. Phys.* **2008**, *128*, 224901 – 224917.
[24] S. W. Homans, *Drug Discovery Today* **2007**, *12*, 534 – 539.
[25] Closer to completion of the $(n\text{-butyrate})_{24}$ assembly, the energetics of ligand exchange might begin to reflect stoichiometric limits imposed by the dimensions of the interior of the capsule. When energies for entry of the 24th *n*-butyrate anion are included, however, the trend in the Figure is simply extended.

